

# IMAGING OF SDSS $Z > 6$ QUASAR FIELDS: GRAVITATIONAL LENSING, COMPANION GALAXIES AND THE HOST DARK MATTER HALOS

CHRIS J. WILLOTT<sup>1</sup>, WILL J. PERCIVAL<sup>2</sup>, ROSS J. MCLURE<sup>2</sup>, DAVID CRAMPTON<sup>1</sup>, JOHN B. HUTCHINGS<sup>1</sup>, MATT J. JARVIS<sup>3</sup>, MARCIN SAWICKI<sup>1</sup>, & LUC SIMARD<sup>1</sup>

*Draft version October 25, 2018*

## ABSTRACT

We have undertaken deep optical imaging observations of three  $6.2 < z < 6.5$  quasar fields in the  $i'$  and  $z'$  filters. These data are used to search for foreground galaxies which are gravitationally lensing the quasars and distant galaxies physically associated with the quasars. Foreground galaxies are found closer than  $5''$  from the lines-of-sight of two of the three quasars. However, the faintness of these galaxies suggests they have fairly low masses and provide only weak magnifications ( $\mu \lesssim 1.1$ ). No convincing galaxies physically associated with the quasars are found and the number of  $i'$ -band dropouts is consistent with that found in random fields. We consider the expected dark matter halo masses which host these quasars under the assumption that a correlation between black hole mass and dark matter halo mass exists. We show that the steepness of the high-mass tail of the halo mass function at this redshift, combined with realistic amounts of scatter in this correlation, lead to expected halo masses substantially lower than previously believed. This analysis can explain the lack of companion galaxies found here and the low dynamical mass recently published for one of the quasars.

*Subject headings:* cosmology: observation – gravitational lensing – quasars: general

## 1. INTRODUCTION

Active supermassive black holes provide a useful means of locating very distant, massive galaxies. Studies of the host galaxies of luminous active galactic nuclei (AGN) at redshifts up to  $z \approx 2$  show they are associated with galaxies with luminous rest-frame-optical stellar populations, corresponding to  $\gtrsim L_*$  (Kukula et al. 2001; Ridgway et al. 2001; Hutchings et al. 2002; Willott et al. 2003a; Dunlop et al. 2003). Furthermore, the strong correlation between black hole mass and stellar bulge luminosity/mass observed locally (Magorrian et al. 1998; Gebhardt et al. 2000; Ferrarese & Merritt 2000) shows that the most massive galaxies are those whose black holes have accreted the greatest mass and therefore were the most luminous AGN.

It is now possible to discover luminous quasars out to a redshift of  $z = 6.4$ . Sources at this redshift are observed as they were  $\approx 13$  Gyr ago (93% of the age of the universe). The Sloan Digital Sky Survey (SDSS) has made a spectacular breakthrough in locating such quasars and now 12 are known at  $z > 5.7$  (Fan et al. 2004). Black hole masses in these quasars are usually estimated by making the assumption that the quasars are accreting at the Eddington limit (e.g. Fan et al. 2001). This method is consistent with a black hole mass measurement from the kinematics of the broad emission line gas (Willott, McLure & Jarvis 2003b). Under the Eddington

argument, the black hole masses of these quasars are mostly in the range  $1 - 5 \times 10^9 M_\odot$ . These black hole masses could be much lower in the case of strong gravitational lensing or beaming. Observations so far have not shown such effects (Fan et al. 2003; Richards et al. 2004; Willott et al. 2003b).

The space density of these luminous SDSS quasars is extremely low,  $\rho = (6.4 \pm 2.4) \times 10^{-10} \text{Mpc}^{-3}$  (Fan et al. 2004). The rarity of these objects and their large black hole masses makes it tempting to associate these quasars with the rarest peaks in the dark matter density distribution (Fan et al. 2001). The dark matter halos hosting the quasars would, under this hypothesis, have a mass of  $> 10^{15} M_\odot$ . Such halos would merge with smaller halos and in the present day would be identified as massive galaxy clusters with a giant elliptical galaxy hosting the dormant supermassive black hole at the bottom of the potential well. However, it is also possible that the SDSS quasars reside in much more common, lower-mass halos and that the correlation between halo mass and black hole mass is not well established at this early epoch. Determining the masses of the quasar host halos is extremely important for understanding the connection between black hole and galaxy growth in the early universe.

The evidence from sub-millimetre observations paints a rather confusing picture. On the one hand, thermal emission from dust has been detected from several of the quasars. These detections imply huge dust masses and star formation rates of several thousand  $M_\odot \text{yr}^{-1}$  (Bertoldi et al. 2003a; Priddey et al. 2003). At this rate, the stellar mass of an  $L_*$  elliptical could be built up in  $\sim 0.1$  Gyr. The clustering of galaxies with such high star formation rates at lower redshift ( $z \sim 3$ ) is not well constrained, but early results suggest these galaxies are associated with massive dark matter halos (Blain et al. 2004, although see Adelberger 2005). One of these quasars, SDSS J1148+5251, has also been detected in molecular carbon monoxide transitions (Bertoldi et al. 2003b; Walter et al. 2003). The CO spectra have a relatively narrow velocity profile with width  $280 \text{ km s}^{-1}$ . Walter et al. (2004) obtained high-resolution imaging of the CO emission and confirm it

<sup>†</sup> Based on observations obtained at the Gemini Observatory, which is operated by the Association of Universities for Research in Astronomy, Inc., under a cooperative agreement with the NSF on behalf of the Gemini partnership: the National Science Foundation (United States), the Particle Physics and Astronomy Research Council (United Kingdom), the National Research Council (Canada), CONICYT (Chile), the Australian Research Council (Australia), CNPq (Brazil) and CONICET (Argentina).

<sup>1</sup> Herzberg Institute of Astrophysics, National Research Council, 5071 West Saanich Rd, Victoria, B.C. V9E 2E7, Canada; chris.willott@nrc.ca, david.crampton@nrc.ca, john.hutchings@nrc.ca, marcin.sawicki@nrc.ca, luc.simard@nrc.ca

<sup>2</sup> Institute for Astronomy, University of Edinburgh, Royal Observatory, Blackford Hill, Edinburgh, EH9 3HJ, UK; wjp@roe.ac.uk, rjm@roe.ac.uk

<sup>3</sup> Astrophysics, Department of Physics, Keble Road, Oxford, OX1 3RH, UK; mjj@astro.ox.ac.uk

comes from a compact structure (a few kpc). These observations allow a dynamical mass estimate for the mass within the central 2.5 kpc of the galaxy. This mass is comparable to the inferred molecular gas mass and is an order of magnitude lower than the mass predicted by assuming that this quasar resides in one of the rare peaks corresponding to dark matter halos of  $> 10^{13} M_{\odot}$ . Although there are some uncertainties in the dynamical mass estimate, particularly the geometry and inclination of the gas, this result casts serious doubt on the belief that the SDSS quasars pinpoint the most massive galaxies at high redshift.

Another approach to determining the mass of the quasar host dark matter halo is via a search for companion galaxies. If the SDSS quasars are formed in the rarest density peaks, then these correspond to large-scale overdense regions and hence the number of dark matter halos located nearby is substantially above the cosmic mean (Kaiser 1984; Barkana & Loeb 2004). Hence the rarest peaks at  $z \approx 6$  are likely to be the sites of the first proto-clusters. If the quasars really do occupy very massive halos, we would expect to see star forming galaxies in their vicinity. To attempt to find these companion galaxies we have carried out deep optical imaging around the three highest redshift quasars from the sample of Fan et al. (2003). In this paper we present these data, describe a search for foreground galaxies which may be gravitationally lensing the quasars and a search for star forming galaxies at the quasar redshift. Finally, we discuss the implications for the host halos of the most distant quasars. Cosmological parameters of  $H_0 = 70 \text{ km s}^{-1} \text{ Mpc}^{-1}$ ,  $\Omega_M = 0.3$  and  $\Omega_{\Lambda} = 0.7$  are assumed throughout.

## 2. OBSERVATIONS

We present observations for three quasars: SDSS J103027.10+052455.0 (SDSS J1030+0524;  $z = 6.30$ ), SDSS J104845.05+463718.3 (SDSS J1048+4637;  $z = 6.20$ ) and SDSS J114816.64+525150.3 (SDSS J1148+5251;  $z = 6.42$ ). The three quasar fields were imaged using the GMOS-North imaging spectrograph on the Gemini-North Telescope. GMOS-North uses an array of three  $2048 \times 4608$  pixel EEV CCD detectors. The pixel scale is  $0.073''$  per pixel giving a useful field-of-view for imaging of  $5.5' \times 5.5'$ . Since the typical seeing size of the observations is in the range  $0.5$  to  $0.7''$ , the pixels were binned by a factor of 2 in both directions to speed up readout and data processing. The observations were carried out in queue mode during November and December 2003. Typical exposure times are  $\approx 2$  hours in the  $z'$ -band and  $\approx 3$  hours in the  $i'$ -band. The relative exposure times were designed to give similar sensitivity in the two bands for very red objects with colours of  $i' - z' \approx 1.5$ . More details of the observations are given in Table 1.

The GMOS-North detectors have significant fringing at the red end of the optical wavelength regime. This is of particular concern for the observations presented here which use the red  $i'$  and  $z'$  filters. The fringe pattern remains constant over time, so the fringes can be successfully removed if one obtains sufficient data to construct a high signal-to-noise fringe frame free of stars and galaxies. To enable the construction of these fringe frames, the observations of each field in each filter were split into 20 to 30 individual frames and the telescope was dithered in a  $3 \times 3$  pattern with offsets of  $10''$  in each direction. Median-combining all the data in each filter from the three fields enabled the construction of fringe frames free of astronomical objects.

Reduction of the imaging data was carried out using stan-

TABLE 1. GMOS-N IMAGING OBSERVATIONS.

Quasar	Band	Exposure time (s)	$3\sigma$ limiting mag (AB)	Seeing ( $''$ )
SDSS J1030+0524	$z'$	8100	26.3	0.68
SDSS J1048+4637	$z'$	5850	26.2	0.61
SDSS J1148+5251	$z'$	7650	26.2	0.65
SDSS J1030+0524	$i'$	9900	27.5	0.65
SDSS J1048+4637	$i'$	12150	27.7	0.54
SDSS J1148+5251	$i'$	13050	27.6	0.67

dard procedures. Most of the reductions were performed using tasks in the IRAF Gemini package which were specifically designed for GMOS. The first step is removal of the bias level using a bias frame constructed from many ( $> 10$ ) bias observations (with the same binning) carried out during the same month. The images were flat-fielded using flat-field frames generated from observations of the twilight sky. The three separate CCD images were then mosaiced together into one large image. The fringe frames generated from all observations within each filter were then scaled and subtracted from each image. All images were then inspected and in some cases a different scaling was applied to better subtract off the fringes. The images were then scaled to correct for atmospheric extinction.

All the images in each filter of the same field were then positionally registered using detected objects and combined into one image rejecting pixels deviating by more than 2.5 sigma from the median and using a bad pixel mask. This method successfully removed CCD defects and cosmic rays whilst not rejecting counts from actual objects. The combined images still showed a low-level, large-scale, residual background which varied across the images. The large-scale background was successfully removed by applying the background subtraction method of the SExtractor software (Bertin & Arnouts 1996) with a mesh size of  $19''$ . The  $i'$  images for each field were then shifted so that objects would appear in the same locations in the  $i'$  and  $z'$  images. Astrometry was performed by using the known geometric distortion of GMOS-North on the sky and setting the positions of the quasar targets to the positions given in the SDSS survey. Photometric calibration was achieved using photometric standard stars observed during the same nights as some of our observations.

## 3. OBJECT DETECTION, PHOTOMETRY AND COMPLETENESS

Detection of objects in the images was performed using the SExtractor software. The  $z'$ -band was selected as the primary detection waveband since  $z > 6$  galaxies are expected to have  $i' - z' > 2$  and may therefore be undetected at  $i'$ . SExtractor was run in ‘‘double-image’’ mode to determine  $i'$ -band measurements for objects detected in  $z'$ . The edges of the images do not contain data at all dither positions and hence have lower sensitivity, contain artifacts and have a varying background. Objects in these regions were excluded from the object catalogues. The useful area of the catalogues is  $27, 27, 28$  square arcmin for SDSS J1030+0524, SDSS J1048+4637 and SDSS J1148+525, respectively.

Magnitudes on the AB system were measured in circular apertures of diameter  $1.5''$ . This size was chosen because it is greater than twice the seeing size, is much greater than the size scales of known  $z > 6$  galaxies (Bouwens et al. 2004) and has lower magnitude errors than larger apertures. Aperture corrections were applied statistically to the  $z'$ -band magnitudes

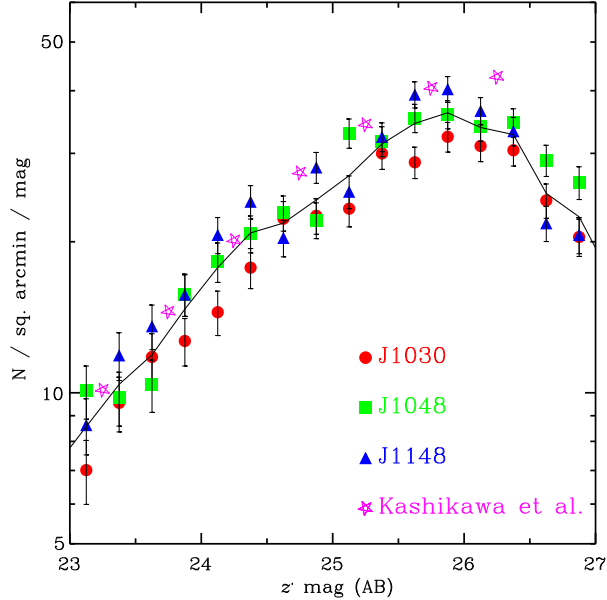


FIG. 1.— Binned number counts in the  $z'$ -band in the fields of the three  $z > 6$  quasars. The  $z'$ -band magnitudes have been aperture-corrected using the prescription given in Sec. 3. Error bars include only Poisson errors. The solid curve is the mean counts averaged over the three fields. The open stars show the  $z'$ -band number counts from the deeper and wider-area Subaru Deep Field (Kashikawa et al. 2004). The counts are consistent given the size of the error bars up to  $z' = 26$ . Beyond  $z' = 26$  the quasar field counts turn over indicating severe incompleteness.

by fitting a linear function to the difference between the total magnitude and aperture magnitude as a function of aperture magnitude. The best-fit relation is  $z'_{\text{total}} - z'_{\text{ap}} = 3.58 - 0.133z'_{\text{ap}}$  which gives an aperture correction of 0.25 mag at  $z' = 25$ . Note that this relation will lead to large aperture corrections at bright magnitudes, which may be inappropriate for compact sources such as stars, but we are in general only interested in faint objects for which the aperture corrections are reasonable ( $z' > 23$ ). A similar procedure was not adopted for the  $i'$ -band magnitudes since the uncorrected aperture magnitudes are used to measure the  $i' - z'$  colours.

The rms noise in the sky background was measured to determine the magnitude limits of the images. Magnitude limits are quoted as  $3\sigma$  limits in  $1.5''$  apertures. Typical magnitude limits are  $z' \approx 26.2$  and  $i' \approx 27.6$  (see Table 1). The relative depths of the images are suitable for detecting very red objects with  $i' - z' > 1.5$ .

To assess the completeness of the  $z'$ -band catalogues we consider both the observed number counts and the recovery of simulated objects. Binned number counts for the  $z'$ -band images for all three fields are shown in Fig. 1. The counts in the three fields do not differ significantly from each other. They agree well with the  $z'$ -band counts determined from a deeper and much larger area survey (0.2 square degrees or thirty times the GMOS-North field-of-view) of the Subaru Deep Field by Kashikawa et al. (2004). The number counts in the quasar fields begin to change slope at  $z' > 25.5$  and turn over at  $z' = 26$ , indicating this is where the sample becomes incomplete.

The source recovery as a function of magnitude was determined by populating the images with artificial galaxies and then using SExtractor to attempt to detect these objects.

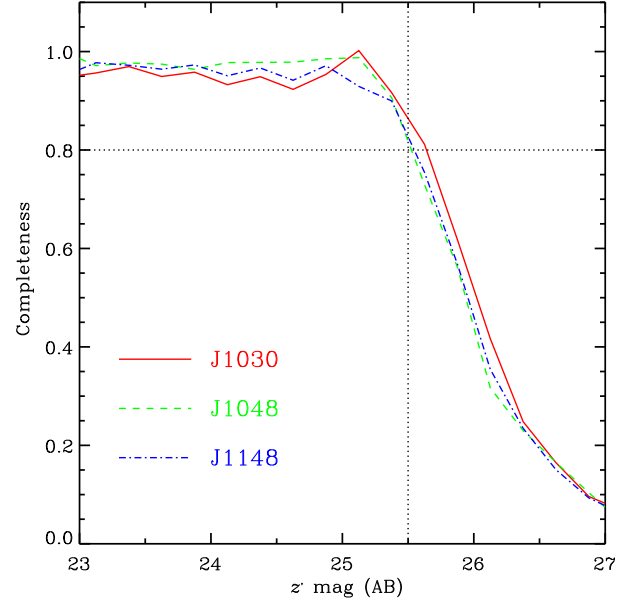


FIG. 2.— Completeness ratio against aperture-corrected  $z'$ -band magnitude derived from recovery of simulated galaxies as detailed in Sec. 3. The curves are quite similar for the three different fields. Dotted lines indicate the location of a completeness ratio of 0.8 and the adopted complete magnitude limit of  $z' = 25.5$ .

About 10 000 artificial galaxies with magnitudes in the range  $23 < z' < 27$  were placed into copies of the  $z'$  images of each quasar. Regions of the images already occupied by objects were masked out of the process to eliminate incompleteness due to blending. SExtractor was run twice: firstly on images containing only the artificial galaxies and a very low noise level and then on the actual quasar field images with the artificial galaxies inserted. The ratio of the number of artificial objects detected in the quasar field images to the number in the low noise images gives the completeness. This completeness ratio is plotted as a function of magnitude for the three quasar fields in Fig. 2. The completeness in all the fields is fairly flat at close to 1 up to  $z' = 25.2$  and then begins to decline. The rapid decline occurs at  $z' > 25.5$  and the completeness drops to 0.5 by  $z = 26.0$ . All the fields have completeness  $> 0.8$  at  $z' = 25.5$  and we adopt this as the magnitude at which completeness begins to become an issue. This analysis with simulated objects agrees well with the results for the number counts discussed previously.

#### 4. SEARCH FOR FOREGROUND GALAXIES LENSING THE QUASARS

The combined effects of a steep luminosity function and the high optical depth to  $z \sim 6$  mean that gravitational lensing is expected to be particularly important for surveys of luminous quasars at high redshift, such as the SDSS  $z > 5.7$  quasar survey. Predictions for the fraction of multiply imaged quasars in the SDSS for various forms of the luminosity function have been made by Wyithe & Loeb (2002a;b) and Comerford, Haiman & Schaye (2002). Fan et al. (2003) and Richards et al. (2004) discuss high-resolution imaging (ranging from  $0.1''$  to  $0.8''$ ) of all seven known  $z > 5.7$  quasars at the time and found that none of them appears to be multiply-imaged. However, the lack of multiple images of the SDSS quasars does not necessarily mean that lensing is unimpor-

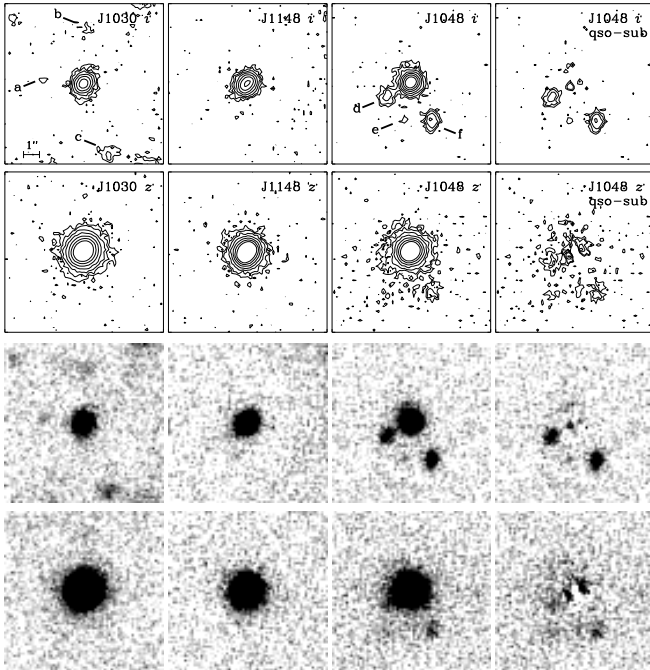


FIG. 3.— GMOS images in the  $i'$ - and  $z'$ -bands centred on the three quasars SDSS J1030+0524, SDSS J1148+5251 and SDSS J1048+4637 (left to right). The final column shows the images of SDSS J1048+4637 after subtracting off a scaled point-spread function at the location of the quasar to show more clearly the nearby galaxies. There are some residuals from the psf-subtraction process which tests on stars in the field show are likely to be artifacts. Each box is  $10''$  on a side, centred on the quasar with north up and east to the left. Contour plots are shown with a logarithmic scale at approximately 1.5, 3, 5, 9, 17, 31,  $56 \times$  the background rms per pixel. Greyscale plots have a linear stretch ranging from  $-0.5 \times$  the background rms (white) to  $+4 \times$  the background rms (black).

tant. For simple singular isothermal sphere models the magnification is  $\mu < 2$  if the source is singly-imaged. More realistic potentials including isothermal ellipsoids, cluster-scale halos and micro-lensing can give rise to higher magnifications for singly-imaged quasars (Keeton, Kuhlen & Haiman 2004; Wyithe & Loeb 2002a).

Shioya et al. (2002) found a faint galaxy close to the line-of-sight of the  $z = 5.74$  quasar SDSS J1044-0125. The lensing galaxy has a magnitude  $i'(AB) = 24.3$ , separation from the quasar  $\theta = 1.9''$  and a likely redshift in the range  $1.5 < z < 2.5$ . Spurred on by this discovery, this group observed two more high-redshift quasar fields (SDSS J1030+0524 at  $z = 6.30$  and SDSS J1306+0356 at  $z = 5.99$ ), but failed to find galaxies projected closer than  $6''$  and  $3''$  to these quasars, respectively (Yamada et al. 2003).

We have imaged three quasar fields and in this section we use our data to search for foreground galaxies which may be lensing the quasars. One of these fields, SDSS J1030+0524, has been imaged before by Yamada et al. (2003), but our images are 1-2 mags deeper and have better resolution than those in Yamada et al. and Shioya et al. Images of the regions surrounding the quasars are shown in Fig. 3. Contours and greyscales are shown for the same fields to highlight different aspects of these high dynamic range images. The contours show smooth isophotes in the quasar flux which rule out the existence of very close, bright companion galaxies and gravitational lensing image splitting in the quasars at the limit of our resolution. The ellipticities and FWHM of the quasars are

TABLE 2. OBJECTS DETECTED WITHIN  $5''$  OF THE QUASARS.

Object	Object position (J2000)	$\theta/''$	$i'$ (AB)	$z'$ (AB)
a	10:30:27.26 +05:24:55.3	2.5	$27.54 \pm 0.35$	$> 26.3$
b	10:30:27.08 +05:24:58.2	3.5	$26.69 \pm 0.17$	$26.12 \pm 0.28$
c	10:30:26.99 +05:24:50.6	4.6	$26.05 \pm 0.10$	$> 26.3$
d	10:48:45.19 +46:37:17.4	1.7	$25.67 \pm 0.05$	$24.97 \pm 0.11$
e	10:48:45.10 +46:37:16.1	2.2	$27.32 \pm 0.22$	$> 26.2$
f	10:48:44.92 +46:37:15.9	2.7	$25.37 \pm 0.04$	$24.82 \pm 0.10$

NOTE. — Objects detected at  $i'$ -band within a  $5''$  radius of the quasars. Three objects were detected in each of the fields of SDSS J1030+0524 and SDSS J1048+4637. Nothing was detected within  $5''$  of SDSS J1148+5251. Object refers to the labels in Fig. 3.  $\theta$  is the separation of the object and the quasar. Magnitudes are given as observed in a  $1.5''$  diameter aperture. Limits at  $z'$ -band are  $3\sigma$  in the same size aperture.

consistent with those of stars in the images.

We searched for objects close to the quasars by inspection of smoothed images. We only consider objects within a  $5''$  radius of the quasars, since lensing by galaxy-sized masses is only effective with impact parameters of a few arcsec. In addition, the probability of finding a galaxy at random within a circle of  $5''$  radius is large at the magnitude limit of the  $i'$ -band images (this probability is 0.9 for  $i' < 27$ ).

Three galaxies were detected in the fields of each of SDSS J1030+0524 (labelled a, b, c) and SDSS J1048+4637 (d, e, f) and none in the field of SDSS J1148+5251. The details of these galaxies are given in Table 2. All of these galaxies are visible in the  $i'$ -band and their  $i' - z'$  colours (or colour limits) show they are foreground to the quasars. For SDSS J1030+0524, the objects are all rather faint ( $i' > 26$ ) and distant from the quasar ( $\geq 2.5''$ ). For SDSS J1048+4637, the closest galaxy (d) is only  $1.7''$  from the quasar. To measure accurate photometry for this galaxy it was necessary to subtract the bright unresolved quasar from the image (far-right panels of Fig. 3). Galaxy d has  $1.5''$  aperture magnitudes of  $i' = 25.67 \pm 0.05$ ,  $z' = 24.97 \pm 0.11$ . The galaxy  $2.7''$  from the quasar (f) has similar magnitudes. Both these galaxies have fairly red colours with  $i' - z' = 0.70$  and  $0.55$ , respectively. Only 20% of galaxies in our images with similar magnitudes have  $i' - z' > 0.5$ .

#### 4.1. Lensing galaxy masses, redshifts and magnifications

In order to determine the lensing magnification due to such galaxies one needs to know the galaxy mass (or equivalently the velocity dispersion) and redshift. Under the simplifying assumption that the lens potential can be modelled as an isothermal sphere the magnification  $\mu$  is  $\mu = \theta/(\theta - \theta_E)$ , where  $\theta$  is the angle from the lens galaxy to the source,  $\theta_E$  is the Einstein radius given by  $\theta_E = 4\pi(\sigma_v/c)^2(D_{LS}/D_{OS})$ , where  $D_{LS}$  is the lens-source angular diameter distance and  $D_{OS}$  is the observer-source angular diameter distance.

Neither the masses nor redshifts are strongly constrained by our photometric observations, but we will use the information available to determine likely values. The red colour of  $i' - z' = 0.70$  for galaxy d close to SDSS J1048+4637 is not consistent with the colour of known galaxies at low redshifts. Therefore we can at least put a lower limit on the redshift of this galaxy. Also, galaxy colours at high redshifts are expected to be blue in the absence of dust reddening, due to the prominence of young stellar populations. We used the HyperZ code (Bolzonella, Miralles & Pelló 2000) with the 2 photometric points to determine if this colour leads to any

constraints on the redshift. Using a range of evolving galaxy templates with moderate dust reddening ( $0 \leq A_V \leq 0.5$ ) we find a 90% confidence range for the redshift is  $0.4 < z < 2.1$ . There is also a secondary solution at  $5.1 < z < 5.5$  where the red colour is due to the Lyman break entering the  $i'$ -band. Considering the redshift distribution of galaxies of this magnitude it is most plausible that the galaxy is at the lower redshift range. Note that if this galaxy is *highly* reddened by dust, then the redshift is no longer well-constrained.

The mass or stellar velocity dispersion of the galaxy can be estimated from the photometry by assuming a redshift and star formation history. Given the red colour of this galaxy we assume that it is an early-type which has undergone passive evolution after a starburst at high redshift and use the evolving elliptical galaxy template from Bruzual & Charlot (2003) which formed at  $z = 7$  (the exact formation redshift assumed does not critically change the results presented here). The correlation between  $i'$ -band absolute magnitude and  $\sigma_v$  observed at low redshifts (Bernardi et al. 2003) was used to relate the evolved absolute magnitude to  $\sigma_v$ . For three possible lens redshifts of  $z = 0.4, 1, 2$  the calculated stellar velocity dispersion is  $\sigma_v = 55, 87, 127 \text{ km s}^{-1}$ . Note that the Bernardi et al. relation is only derived for  $z < 0.3$  and  $\sigma_v > 100 \text{ km s}^{-1}$ , so its use here involves extrapolation in both redshift and velocity dispersion. Given the redshift of the source is  $z = 6.20$  and  $\theta = 1.7''$  this leads to Einstein radii  $\theta_E = 0.07, 0.13, 0.18''$  and magnifications  $\mu = 1.04, 1.08, 1.12$  for lens redshifts of  $z = 0.4, 1, 2$ , respectively.

It is clear that, whatever the redshift of this lensing galaxy, it is not very massive and provides only a small magnification to the flux of SDSS J1048+4637. Therefore it makes a negligible difference to the derived luminosity and black hole mass. Given that the closest galaxy to SDSS J1030+0524 (galaxy a) is even fainter and further away, the magnification in that case will be even lower. An increase in the magnification could come about if (i) the galaxy lies in a moderately rich high-redshift cluster; or (ii) the galaxy resides in a dark matter halo with higher than average mass-to-light ratio.

For SDSS J1044-0125, Shioya et al. (2002) estimated the lens galaxy to have a velocity dispersion of  $\sigma_v \sim 200 \text{ km s}^{-1}$  and be located at redshift  $z \approx 2$ . According to Shioya et al. this would give a magnification of  $\mu = 2$ . However we have repeated their calculations and find their values for the Einstein radius and magnification to be erroneous (this error is also present in Yamada et al. 2003). For  $z = 2$  and  $\sigma_v = 200 \text{ km s}^{-1}$ , the magnification is actually  $\mu = 1.3$ . The range of plausible lens redshift and velocity dispersion combinations given in their paper lead to a range of  $1.1 < \mu < 1.5$ . As with SDSS J1048+4637, the corrections to the derived luminosity and black hole mass of SDSS J1044-0125 are small.

##### 5. SEARCH FOR $Z > 6$ GALAXIES IN THE QUASAR FIELDS

Galaxies at redshifts  $z > 5.7$  can be identified by the sharp drop in flux across the Lyman break leading to a very red  $i' - z'$  colour. The  $z > 6$  SDSS quasars have  $z' \approx 20$  and colours measured from our images of  $i' - z' = 3.25, 2.98, 3.25$  respectively for SDSS J1030+0524, SDSS J1048+4637 and SDSS J1148+5251. The spectra of quasars and star forming galaxies over the rest-frame wavelength range 90–140 nm probed by the  $i'$  and  $z'$  filters are dominated by a large break due to absorption by neutral hydrogen. Therefore one would expect companion galaxies to have comparable  $i' - z'$  colours to the quasars. The fact that the light from a companion galaxy would pass through IGM neighbouring that which

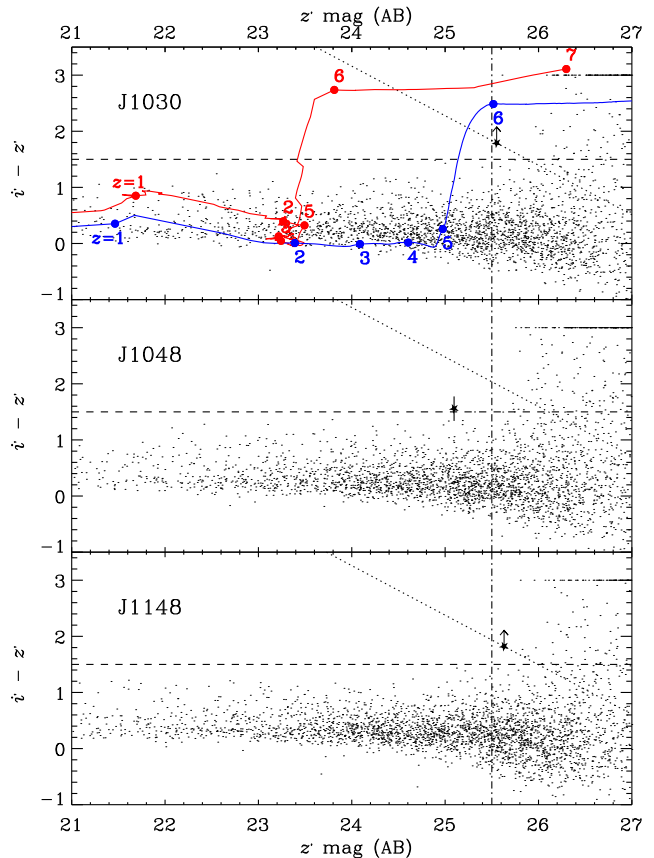


FIG. 4.— Colour-magnitude (aperture-corrected) diagrams for objects detected in  $z'$  in the quasar fields. The completeness limit of  $z' = 25.5$  is shown with a dot-dashed line. The high-redshift galaxy selection criterion of  $i' - z' > 1.5$  is marked with the dashed line. The dotted line represents the colour of an object which is just detected at the  $3\sigma$  level in the  $i'$ -band as a function of the  $z'$ -band magnitude. Most objects with measured zero or negative flux in the  $i'$ -band are plotted at  $i' - z' = 3$ . The exceptions to these are objects which pass the  $i'$ -band dropout selection criteria discussed in Sec. 5. These are shown with star symbols and lower limits on the  $i'$ -band  $3\sigma$  line. The dots at  $i' - z' > 1.5$  indicate sources which are detected at less than  $4\sigma$  at  $z'$ -band and hence have very large uncertainties on their magnitudes and colours and in some cases may be spurious. The labelled curves show the colour and magnitude as a function of redshift for an evolving  $L^*$  elliptical (upper curve) and a non-evolving  $L^*$  Lyman-break galaxy (lower curve) – see text for more details.

the quasar light passes through, further strengthens the idea that the colours of companion galaxies are expected to be  $i' - z' \approx 3$ .

Simulated colour-magnitude tracks for two different types of galaxy as a function of redshift are shown on Fig. 4. Model galaxy spectra were generated from the Bruzual & Charlot (2003) spectral synthesis code with Lyman forest absorption evolution matching the observations of Songaila & Cowie (2002). The upper curve is a present-day  $L^*$  elliptical which formed all of its stars in a starburst starting at  $z = 10$  with a characteristic timescale of 1 Gyr and evolved since without merging. There is no dust extinction assumed for this model, but in reality the dust extinction would increase with redshift (due to evolution and  $k$ -correction) making the galaxy redder and fainter than plotted at higher redshifts. The lower curve is a  $L^*$  Lyman-break galaxy model where the galaxy is observed 0.5 Gyr into a constant star formation rate starburst. It is clear that the only possible low-redshift contaminants with  $i' - z' > 1.5$  are galaxies with a high level of dust reddening.

Also plotted on Fig. 4 are colour-magnitude diagrams constructed from the  $z'$ -band-selected catalogues described in Sec. 3 for each of the three quasar fields. Most objects have colours in the range  $0 < i' - z' < 1$  as is well known from previous surveys (Dickinson et al. 2004; Capak et al. 2004). These colours are in agreement with the model galaxy tracks at  $z < 5$ .

A search was made for objects which could plausibly be high-redshift galaxies. The  $i'$ -band dropout selection criteria adopted were signal-to-noise ratio in the  $z'$ -band  $\geq 4$  and a colour of  $i' - z' \geq 1.5$ . Possible candidates were inspected and magnitudes checked to ensure their unusual colours are not spurious. A total of three objects satisfying these criteria were found - these are shown with filled symbols on Fig. 4. These all have magnitudes in the range  $25 < z' < 26$  and only one of them is detected at the  $3\sigma$  level at  $i'$ -band. This object has  $z' = 25.10$  and a colour of  $i' - z' = 1.56 \pm 0.22$ . The other two objects have  $z' \approx 25.6$  and only lower limits on their  $i' - z'$  colours which lie in the range  $1.7 - 1.9$ .

In Sec. 3 we showed that our  $z'$ -band images are complete at the greater than 80% level to  $z' = 25.5$ . Fig. 4 shows that at  $z' \leq 25.5$ , every single  $z'$ -band object detected on our images has a counterpart at the  $> 3\sigma$  level in the  $i'$ -band image. At fainter magnitudes, this is no longer true and our constraints on the  $i' - z'$  colours of objects at these magnitudes becomes very weak due to uncertainty in both the  $z'$  and  $i'$  magnitudes. Therefore we will limit further analysis to objects brighter than the magnitude limit of  $z' = 25.5$ .

At  $z' < 25.5$  we find one  $i'$ -band dropout in the three quasar fields. This object has  $i' - z' = 1.56 \pm 0.22$  which is quite close to the colour selection value and the size of the uncertainty means it is quite plausible that photometric errors have scattered the colour into the dropout range. The measured colour is about  $7\sigma$  away from the colours of the SDSS quasars, which suggests that if it is a high-redshift galaxy, then it is most likely foreground to the quasars with a redshift in the range  $5.7 < z < 6$ . The galaxy is located a projected distance of  $81''$  from the quasar (approximately halfway from the quasar to the edge of the GMOS field). Therefore we conclude that there are no plausible galaxies brighter than  $z' = 25.5$  associated with any of these three quasars.

We now consider the number of  $i'$ -band dropouts we could have expected to find under the assumption that the quasar fields are “random” and show no enhancement due to the existence of the quasars. The best comparison datasets which go deep enough over a wide area are the *Hubble Space Telescope* ACS imaging of the GOODS regions (Giavalisco et al. 2004) and the Subaru Deep Field (Kashikawa et al. 2004). These observations give a surface density of objects with  $z' < 25.5$  and  $i' - z' > 1.5$  of  $0.01 - 0.02 \text{ arcmin}^{-2}$  (Dickinson et al 2004; Bouwens et al. 2004; Nagao et al. 2004). The total sky area we have surveyed with GMOS-North is  $82 \text{ arcmin}^2$ . Therefore on the basis of the GOODS and SDF observations we would expect  $\approx 1 - 2$   $i'$ -band dropouts in our total area. Our finding of one dropout is entirely consistent with the expectations for a blank field.

The results presented in this section show that these quasar fields do not exhibit an excess of luminous companion galaxies. The magnitude limit of  $z' = 25.5$  corresponds to a UV luminosity of  $L_{1500} = 2.5 \times 10^{29} \text{ ergs}^{-1} \text{ Hz}^{-1}$  at a redshift of  $z = 6.3$ . This is equivalent to  $2L^*$  in the  $z \approx 6$  galaxy luminosity function (Bunker et al. 2004) and an unobscured star formation rate of  $SFR = 30 M_{\odot} \text{ yr}^{-1}$ , assuming the con-

version given in Madau, Pozzetti & Dickinson (1998). The few known galaxies at redshifts  $z \approx 6.6$  discovered in narrow-band surveys have star formation rates derived from their UV luminosities comparable to this limit (Hu et al. 2002; Kodaira et al. 2003). For comparison, the millimeter detections of dust in SDSS J1048+4637 and SDSS J1148+5251 imply total star formation rates  $> 1000 M_{\odot} \text{ yr}^{-1}$  in the host galaxies of the quasars (Bertoldi et al. 2003a).

A similar study to ours has recently been reported by Stiavelli et al. (2005). They have observed the quasar SDSS J1030+0524 with ACS on the *Hubble Space Telescope* in the  $i_{775}$  and  $z_{850}$  filters. Their data reaches slightly deeper than ours and they identify seven objects with  $i_{775} - z_{850} > 1.5$  in the quasar field. Only 3% of randomly-selected areas in the GOODS fields show such a high density of red objects, indicating an excess in the field of this quasar. The single  $i' - z' > 1.5$  object we discovered in the field of SDSS J1030+0524 which is plotted on Fig. 4 is also found by Stiavelli et al. and a high-resolution image of it is shown in the upper panel of their Fig. 2. Four of the seven objects found with ACS are detected at  $i_{775}$  and have  $i_{775} - z_{850} < 2$ . These objects are not red enough to be located at a redshift similar to the quasar (Dickinson et al. 2004). A spectroscopic redshift has been obtained for one object and it reveals a redshift of  $z = 5.970$ . The large redshift difference between the quasar and this galaxy means that if they are part of the same large-scale overdensity then the comoving scale of that structure is larger than anything found in the low-redshift universe (Pandey & Bharadwaj 2005).

## 6. CONSTRAINTS ON THE DARK MATTER HALO MASSES

Early-type galaxies in rich clusters in the local universe show homogeneous, old stellar populations suggesting coeval star formation at high redshifts (e.g. López-Cruz, Barkhouse & Yee 2004). Therefore, if the quasars (two of which have far-IR luminosities indicating vigorous star formation) are in proto-cluster environments one would expect to see massive companion galaxies forming stars. It has been suggested that there could be a suppression of star formation in the vicinity of a strong UV photo-ionizing field such as that of a quasar (Couchman & Rees 1986). This is because the radiation would heat the diffuse gas in the IGM to a temperature of  $T \sim 1000 \text{ K}$  and inhibit the cooling process by which gas condenses to form stars. However, these effects are likely to be significant only in low mass halos and will not be such an issue for the more massive halos hosting galaxies with  $SFR > 30 M_{\odot} \text{ yr}^{-1}$  which we are sensitive to.

The goal of our observations was to constrain the masses of the dark matter halos hosting these quasars by considering the clustering of star forming galaxies around them. In fact, we have been unable to identify any companion galaxies suggesting that these quasars may not be residing in the most massive halos at this epoch, in line with the dynamical mass measurement of the host galaxy of SDSS J1148+5251 by Walter et al. (2004). However, given the large uncertainties in transforming from observable quantities such as UV star formation rate to typical Lyman break halo mass and duty cycle at  $z > 6$ , it is difficult to directly turn our non-detection into a robust upper limit for the halo masses. In this Section we show that scatter in the  $M_{BH} - M_{DM}$  relation, combined with a steeply falling mass function, biases the host halo masses of the observed high-redshift quasars to lower values, suggesting that the inferred low host halo masses do not necessarily imply a break-down of the low redshift  $M_{BH} - M_{DM}$  correlation at

$z > 6$ .

An upper limit on the halo mass hosting luminous quasars can be calculated from a comparison of their space densities. This method assumes that quasars reside in the most massive halos which exist in sufficient quantity to host all the observed quasars. The nine luminous quasars at redshift  $5.7 < z < 6.5$  discovered by the SDSS (which all have black holes with mass  $M_{\text{BH}} = 1 - 4 \times 10^9 M_{\odot}$  via the Eddington argument) give a space density of  $(6.4 \pm 2.4) \times 10^{-10} \text{Mpc}^{-3}$  (Fan et al. 2004)<sup>5</sup>. The halo mass function at  $z = 6.3$  was determined from the mass function fit to the numerical simulations of Sheth & Tormen (1999). The quasar space density corresponds to the space density of all halos with  $M_{\text{DM}} > 1.5 \times 10^{13} M_{\odot}$ . This limit is cosmology dependent, and is obviously strongly dependent on the high mass tail of the Sheth & Tormen mass function, which is only relatively sparsely sampled in the simulations used to determine this fit. However, in support of this functional form, Barkana & Loeb (2004) show that the tail provides a good approximation to the numerical mass function at extremely high redshifts, provided that the lack of large scale modes in the simulations is taken into account.

An estimate of the host halo masses can be found by using the estimated black hole masses and further assuming that there is a correlation between black hole and halo masses. Such a correlation has been shown to exist at low redshifts (Ferrarese 2002) via a combination of the well known stellar bulge–black hole mass correlation and a correlation between halo circular velocity and bulge velocity dispersion. The correlation determined by Ferrarese (2002) with a correction applied by Bromley et al. (2004) is:

$$\frac{M_{\text{BH}}}{10^8 M_{\odot}} \sim 0.015 \left( \frac{M_{\text{DM}}}{10^{12} M_{\odot}} \right)^{1.82}. \quad (1)$$

The universality of this correlation is untested and in particular whether it evolves with redshift is highly uncertain. We will refer to this non-evolving correlation between  $M_{\text{BH}}$  and  $M_{\text{DM}}$  as case A.

Wyithe & Loeb (2003) have noted that in feedback-regulated black hole growth models (e.g. Silk & Rees 1998; Fabian 1999) the important parameter for the strength of the dark matter halo potential is the circular velocity, not the mass. The relationship between circular velocity and mass is redshift-dependent due to the universal expansion:  $v_c \propto M_{\text{DM}}^{1/3} (1+z)^{1/2}$  (e.g. Barkana & Loeb 2001). The feedback-regulated model of Wyithe & Loeb<sup>6</sup> leads to a redshift-dependent correlation between  $M_{\text{BH}}$  and  $M_{\text{DM}}$  of

$$\frac{M_{\text{BH}}}{10^8 M_{\odot}} \sim f \left( \frac{M_{\text{DM}}}{10^{12} M_{\odot}} \right)^{5/3} (1+z)^{5/2}. \quad (2)$$

Since the dormant black holes observed in the local universe typically formed at redshifts  $1 < z < 2$  (e.g. Yu & Tremaine 2002) we fix the normalizing factor  $f$  so that the correlation roughly matches that of Bromley et al. (2004) at  $z = 1.5$ . This condition is met by  $f = 0.0018$ . We will refer to this evolving correlation between  $M_{\text{BH}}$  and  $M_{\text{DM}}$  as case B.

<sup>5</sup> We neglect the likely existence of quasars just as powerful as those in the SDSS which have their UV luminosities substantially decreased by dust. The space density of obscured quasars at lower redshifts is comparable to that of unobscured quasars (Zheng et al. 2004). However the ratio of obscured to unobscured quasars at  $z = 6$  is so uncertain that we do not attempt to make any correction to the quasar space density.

<sup>6</sup> We omit the parameter  $[\xi(z)]^{5/6}$  from the equation given in Wyithe & Loeb (2003) since it is close to unity and negligible compared with the uncertainties involved.

Since the two possible scenarios are normalized to each other at  $z = 1.5$ , at higher redshifts the host halo for a black hole of a given mass will be less massive for case B than case A. Specifically, for a quasar at  $z = 6.3$  with  $M_{\text{BH}} = 2 \times 10^9 M_{\odot}$ , then case A gives  $M_{\text{DM}} = 5.2 \times 10^{13} M_{\odot}$  and case B gives  $M_{\text{DM}} = 1.3 \times 10^{13} M_{\odot}$ . A simple comparison of the case A estimate with the space-density limit shows that there are insufficient halos with masses of  $M_{\text{DM}} = 5 \times 10^{13} M_{\odot}$  at these high redshifts to host the number of observed quasars. The simple conclusion to draw is that the correlation between black hole mass and halo mass does not remain the same at  $z > 6$  as it is locally. A similar conclusion was reached by Bromley et al. (2004) by considering the total black hole mass density built up by quasars. Wyithe & Loeb (2005) showed that the evolution in the 2dF quasar correlation function over the (admittedly narrow) range  $1 < z < 2$  was more consistent with the evolving  $M_{\text{BH}} - M_{\text{DM}}$  correlation than the redshift-independent one. In what follows we will use both case A and B correlations, whilst remembering that prior evidence supports case B over A.

An important ingredient in the application of such correlations that is often overlooked is the effect of intrinsic scatter in the relation. We now incorporate the scatter in these correlations to estimate the expected host halo masses. We will show that including the scatter makes a significant difference due to the steepness of the halo mass function for these rare halos. This is because lower mass halos are much more abundant, so low mass halos which are outliers in the  $M_{\text{BH}} - M_{\text{DM}}$  correlation could be more abundant than high mass halos on the correlation.

We begin with the dark matter halo mass function fit of Sheth & Tormen (1999). This is evaluated at a redshift of  $z = 6.3$ . Above a mass of  $\sim 10^{12} M_{\odot}$ , the mass function is exponentially declining. The black hole mass within each halo is given by the case A or B correlations. We now add scatter to these black hole masses. The intrinsic scatter in the correlation between black hole mass and stellar velocity dispersion at low redshift is in the range 0.25–0.30 dex (Tremaine et al. 2002). The conversion from stellar velocity dispersion to halo mass is likely to add in considerably more scatter, so we consider 0.4 dex to be the minimum amount of scatter in this correlation at low redshift. This scatter may increase substantially at higher redshifts, particularly for galaxies which are in the process of growing their black holes or accreting matter from the surrounding IGM. To bracket the uncertainty in the scatter we consider four different cases with 0.4, 0.6, 0.8 and 1.0 dex scatter in the correlation. Although the shape of the scatter is unknown even locally, we will adopt a lognormal distribution as the simplest shape.

By identifying the most luminous  $z \sim 6$  quasars across a large fraction of the sky, the SDSS has selected the most massive, active black holes at this epoch (under the assumption that luminous quasars at such early times are accreting at the Eddington limit). Therefore we take a black hole mass cut of  $M_{\text{BH}} > 10^9 M_{\odot}$  and then calculate the probability distribution of dark matter halos which host such massive black holes given the correlations A and B and the various amounts of scatter in the correlation. The results are shown in Fig. 5. Including scatter has considerably decreased the expected masses of the halos hosting these quasars. Even for the case with minimum scatter there is a shift of  $\sim 0.5$  in  $\log_{10} M_{\text{DM}}$ . For the maximum scatter case considered, this shift in  $\log_{10} M_{\text{DM}}$  is  $\sim 1.5$ .

Walter et al. (2004) use resolved CO emission to measure

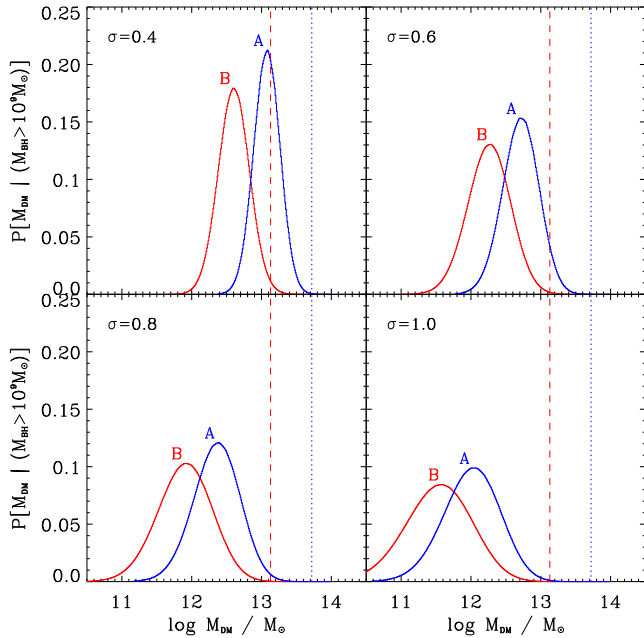


FIG. 5.— Probability distribution for the mass of the dark matter halo hosting a black hole with mass  $> 10^9 M_{\odot}$  at  $z = 6.3$ . These curves were generated assuming correlations between  $M_{\text{BH}}$  and  $M_{\text{DM}}$  of the form A and B (see text) with lognormal intrinsic dispersion  $\sigma$ . The vertical dotted (dashed) line shows the case A (B)  $M_{\text{DM}}$  expected for  $M_{\text{BH}} = 2 \times 10^9 M_{\odot}$  without considering the combined effects of scatter and the steepness of the halo mass function. These plots clearly show that the expected halo masses are considerably lower than obtained by simply using the  $M_{\text{BH}} - M_{\text{DM}}$  correlation without scatter.

a dynamical mass for the inner 2.5 kpc of SDSS J1148+5251 to be  $\sim 5 \times 10^{10} M_{\odot}$ . They argued this to be at least a factor of 10 lower than expected by naive extrapolation of the low redshift correlation between black hole mass and stellar velocity dispersion. We have shown here that using the case B redshift-dependent correlation and/or including the effects of a reasonable amount of scatter ( $\sigma \gtrsim 0.6$ ) lead to an expected halo mass at least an order of magnitude lower than using the naive correlation of case A. This provides a simple explanation for the observations of Walter et al. and those presented

in this paper, without the need for the  $M_{\text{BH}} - M_{\text{DM}}$  correlation to break down at high redshift. A consequence of this is that the SDSS quasars may not be identifying the most overdense regions of the high- $z$  universe as is commonly assumed.

## 7. SUMMARY

We have presented deep imaging in the  $i'$  and  $z'$  filters of the fields of three of the most distant known quasars. For two of the three quasars, there are foreground galaxies at projected distances of a few arcsec. However, the faintness of these galaxies suggests they have relatively low masses which, combined with the large impact parameters, provide only a weak gravitational lensing magnification that would not significantly alter the derived quasar luminosities.

A search for star forming galaxies at the redshifts of the quasars was carried out. No enhancement in Lyman-break galaxies above that in random fields is found. The UV continuum star formation limit reached is  $30 M_{\odot} \text{yr}^{-1}$ , comparable with known  $z \approx 6.5$  galaxies. The lack of companion galaxies could be indicative of these quasars residing in lower mass dark matter halos than previously believed. We consider the effect of scatter in correlations between black hole mass and halo mass and find that this scatter means that we expect the most massive black holes to be found in a range of halo masses, typically much lower than found by use of a simple correlation between the two quantities.

To obtain a more accurate estimate of any overdensity of star forming companions will require much deeper data. Whilst few-orbit ACS observations are able to find a few possible companions (Stiavelli et al. 2005), a proper census requires something of similar depth to the Hubble Ultra Deep Field (reaching  $0.1 L^*$  in the  $z = 6$  galaxy luminosity function with a limiting magnitude of  $z' = 29$ ; Bunker et al. 2004) and such observations will therefore require a large increase in sensitivity such as from the *James Webb Space Telescope*.

Thanks to the Gemini-North queue observers for executing the observations presented here. We thank Stuart Wyithe and Meghan Gray for interesting discussions. Thanks to the anonymous referee for some useful suggestions to improve the paper.

## REFERENCES

- Adelberger K. 2005, ApJ, in press, astro-ph/0412397  
 Barkana, R., Loeb, A. 2001, Phys. Rep., 349, 125  
 Barkana, R., Loeb, A. 2004, ApJ, 609, 474  
 Bernardi, M., et al. 2003, AJ, 125, 1849  
 Bertin, E., Arnouts, S. 1996, A&AS, 117, 393  
 Bertoldi, F., Carilli, C. L., Cox, P., Fan, X., Strauss, M. A., Beelen, A., Omont, A., Zylka, R. 2003a, A&A, 406, L55  
 Bertoldi, F., et al. 2003b, A&A, 409, L47  
 Blain, A. W., Chapman, S. C., Smail, I., Ivison, R. J. 2004, ApJ, 611, 725  
 Bolzonella M., Miralles J.-M., Pelló R. 2000, A&A 363, 476  
 Bouwens, R. J., et al. 2004, ApJ, 606L, 25  
 Bromley, J. M., Somerville, R. S., Fabian, A. C. 2004, MNRAS, 350, 456  
 Bruzual, G., Charlot, S. 2003, MNRAS, 344, 1000  
 Bunker, A. J., Stanway, E. R., Ellis, R. S., McMahon, R. G. 2004, MNRAS, 355, 374  
 Capak, P., et al. 2004, AJ, 127, 180  
 Comerford, J. M., Haiman, Z., Schaye, J. 2002, ApJ, 580, 63  
 Couchman, H. M. P., Rees, M. J. 1986, MNRAS, 221, 53  
 Dickinson, M., et al. 2004, ApJ, 600, L99  
 Dunlop, J. S., McLure, R. J., Kukuła, M. J., Baum, S. A., O'Dea, C. P., Hughes, D. H. 2003, MNRAS, 340, 1095  
 Fabian, A. C. 1999, MNRAS, 308L, 39  
 Fan, X., et al. 2000, AJ, 120, 1167  
 Fan, X., et al. 2001, AJ, 122, 2833  
 Fan, X., et al. 2003, AJ, 125, 1649  
 Fan, X., et al. 2004, AJ, 128, 515  
 Ferrarese, L. 2002, ApJ, 578, 90  
 Ferrarese, L., Merritt, D. 2000, ApJ, 539, L9  
 Gebhardt, K., et al. 2000, ApJ, 539, L13  
 Giavalisco, M., et al. 2004, ApJ, 600, L93  
 Hu, E. M., et al. 2002, ApJ, 568, L75  
 Hutchings, J. B., Frenette, D., Hanisch, R., Mo, J., Dumont, P. J., Redding, D. C., Neff, S. G. 2002, AJ, 123, 2936  
 Kaiser, N. 1984, ApJ, 284, L9  
 Kashikawa, N., et al. 2004, PASJ, 56, 1011  
 Keeton, C. R., Kuhlen, M., Haiman, Z. 2004, ApJ, submitted, astro-ph/0405143  
 Kodaira, K., et al. 2003, PASJ, 55L, 17  
 Kukuła, M. J., Dunlop, J. S., McLure, R. J., Miller, L., Percival, W. J., Baum, S. A., O'Dea, C. P. 2001, MNRAS, 326, 1533  
 López-Cruz, O., Barkhouse, W. A., Yee, H. K. C. 2004, ApJ, 614, 679  
 Priddey, R. S., Isaak, K. G., McMahon, R. G., Robson, E. I., Pearson, C. P. 2003, MNRAS, 344L, 74  
 Madau, P., Pozzetti, L., Dickinson, M. 1998, ApJ, 498, 106  
 Magorrian, J., et al. 1998, AJ, 115, 2285  
 Nagao, T., et al. 2004, ApJ, 613L, 9  
 Pandey, B., Bharadwaj, S. 2005, MNRAS, 357, 1068  
 Richards, G. T., et al. 2004, AJ, 127, 1305



- Ridgway, S. E., Heckman, T. M., Calzetti, D., Lehnert, M. 2001, *ApJ*, 550, 122
- Sheth, R. K., Tormen, G. 1999, *MNRAS*, 308, 119
- Shioya, Y., et al. 2002, *PASJ*, 54, 975
- Silk, J., Rees, M. J. 1998, *A&A*, 331L, 1
- Songaila, A., Cowie, L. L. 2002, *AJ*, 123, 2183
- Stiavelli, M., et al. 2005, *ApJL*, 622, in press
- Tremaine, S., et al. 2002, *ApJ*, 574, 740
- Walter, F., et al. 2003, *Nature*, 424, 406
- Walter, F., Carilli, C., Bertoldi, F., Menten, K., Cox, P., Lo, K. Y., Fan, X., Strauss, M. 2004, *ApJ*, 615L, 17
- Willott, C. J., Rawlings, S., Jarvis, M. J., Blundell, K. M. 2003a, *MNRAS*, 339, 173
- Willott, C. J., McLure, R. J., Jarvis, M. J. 2003b, *ApJ*, 587, L15
- Wyithe, J. S. B., Loeb, A. 2002a, *ApJ*, 577, 57
- Wyithe, J. S. B., Loeb, A. 2002b, *Nature*, 417, 923
- Wyithe, J. S. B., Loeb, A. 2003, *ApJ*, 595, 614
- Wyithe, J. S. B., Loeb, A. 2005, *ApJ*, 621, 95
- Yamada, S. F., et al. 2003, *PASJ*, 55, 733
- Yu, Q., Tremaine, S. 2002, *MNRAS*, 335, 965
- Zheng, W., et al. 2004, *ApJS*, 155, 73